

AdjointDPM: Adjoint Sensitivity Method for Gradient Backpropagation of Diffusion Probabilistic Models

Jiachun Pan*

National University of Singapore
pan.jiachun@u.nus.edu

Jun Hao Liew

ByteDance
junhao.liew@bytedance.com

Vincent Y. F. Tan

National University of Singapore
vtan@nus.edu.sg

Jiashi Feng

ByteDance
jshfeng@bytedance.com

Hanshu Yan*[†]

ByteDance
hanshu.yan@bytedance.com

Abstract

Existing customization methods require access to multiple reference examples to align pre-trained diffusion probabilistic models (DPMs) with user-provided concepts. This paper aims to address the challenge of DPM customization when the only available supervision is a differentiable metric defined on the generated contents. Since the sampling procedure of DPMs involves recursive calls to the denoising UNet, naïve gradient backpropagation requires storing the intermediate states of all iterations, resulting in extremely high memory consumption. To overcome this issue, we propose a novel method AdjointDPM, which first generates new samples from diffusion models by solving the corresponding probability-flow ODEs. It then uses the adjoint sensitivity method to backpropagate the gradients of the loss to the models' parameters (including conditioning signals, network weights, and initial noises) by solving another augmented ODE. To reduce numerical errors in both the forward generation and gradient backpropagation processes, we further reparameterize the probability-flow ODE and augmented ODE as simple non-stiff ODEs using exponential integration. Finally, we demonstrate the effectiveness of AdjointDPM on three interesting tasks: converting visual effects into identification text embeddings, finetuning DPMs for specific types of stylization, and optimizing initial noise to generate adversarial samples for security auditing.

1 Introduction

Diffusion Probabilistic Models (DPMs) constitute a family of generative models that diffuse data distributions into white Gaussian noise and then revert the stochastic diffusion process to synthesize new contents [12, 31]. DPM-based methods have recently achieved state-of-the-art performances in generating various types of contents, such as images [28, 26, 24], videos [2, 36, 13], and audio data [17, 29]. To promote the development of downstream applications that require creativity [7, 4, 15, 27], several pre-trained high-performance models, such as Stable Diffusion (SD) [26], have also been made publicly available.

*Equal contribution. This work was completed during Jiachun Pan's internship at ByteDance.

[†]Project Lead.

Researchers have developed many controllable and customized generation algorithms based on these public models [6, 33, 7, 27, 21]. However, when adapting pre-trained DPMs to customized generation, most existing works [7, 33, 16, 27] require collecting a set of samples with a certain common property (e.g., the same identity, style, or visual effect) to define the desired concept and to finetune the models' parameters. These parameters generally include the conditioning signal (e.g., text embedding) and the trainable weights of the denoising UNet, as they both affect the generation dynamics. Some methods, such as Textual-Inversion [7], try to optimize a unique identifier text embedding to fit a set of images with the same identity. The DPM can then use the obtained identifier to synthesize unseen images of the provided identity. Other methods, such as DreamBooth [27], finetune the weights of a pre-trained image DPM for customization. To ensure the learned parameters can represent the target property and generalize well, these works usually require collecting enough samples or designing dedicated regularization tricks. However, in some cases, it is difficult or even not possible to collect enough data that can represent abstract requirements imposed on the generated content.

In this paper, we address the general problem of *customizing DPMs based on a computable metric evaluated on the generated contents, where the metric can be manually designed even without collecting a set of data samples*. For instance, in image style transfer, one may optimize a plug-in conditioning text token or slightly fine-tune the model's weights, where stylization is defined by the Gram matrix [8] computed from a single reference image's features. Alternatively, one may evaluate the security of a generation system with a content moderation mechanism by optimizing an initial noise \mathbf{x}_T such that its corresponding generated image will mislead the NSFW (not safe for work) classifier while still being visually NSFW. Denote the DPM as $\Phi(\cdot, \cdot, \epsilon_\theta)$, which generates samples by iteratively calling function ϵ_θ . All the above problems can be formulated as an optimization problem that minimizes the loss function $L(\cdot)$ computed based on the generated contents $\mathbf{x}_0 = \Phi(\mathbf{x}_T, c, \epsilon_\theta)$ by optimizing the related variables of Φ , including the weights θ , conditioning signal c , or initial noise \mathbf{x}_T :

$$\min_{\psi \in \{\mathbf{x}_T, c, \theta\}} L(\Phi(\mathbf{x}_T, c, \epsilon_\theta)). \quad (1)$$

To solve the optimization problem, an effective backpropagation (BP) technique is required to compute the gradient of the loss function $L(\mathbf{x}_0)$ with respect to the optimization input variables. Song et al. [31] showed that the DPM sampling process can be solved by solving a probability-flow ODE, and many efficient sampling methods have been developed using adaptive ODE solvers. The sampling process involves recursive calls to the denoising UNet $\epsilon_\theta(\mathbf{x}_t, t, c)$ for multiple iterations. However, naive gradient BP requires intermediate state storage for all iterations, resulting in significant GPU memory consumption. To overcome this problem, we propose AdjointDPM, a novel gradient BP technique based on the adjoint sensitivity method [3]. AdjointDPM computes the gradient by solving a backward ODE that only needs to store the intermediate state at the time point of function evaluation, resulting in constant memory usage. Moreover, we reparameterize the diffusion generation process to a simple non-stiff ODE using exponential integration, which helps reduce discretization errors in both the forward and reverse processes of gradient computation.

We apply AdjointDPM to three interesting tasks involving optimizing the conditioning signal, weights, and initial noise, respectively. In all the tasks, the metrics are all manually designed, e.g., a classifier, the distance between a stylized Gram Matrix. The results demonstrate the flexibility and general applicability of AdjointDPM: 1) AdjointDPM manages to optimize a unique special text embedding # that can control a Stable Diffusion model to synthesize images with certain visual effects (e.g., bokeh and relighting). 2) AdjointDPM can finetune a Stable Diffusion model for stylization defined by a Gram Matrix of a single reference image. 3) We also can use AdjointDPM to audit the security of image generation systems. AdjointDPM successfully synthesizes images with NSFW content, and those images sneakily bypass the moderation filters. This triggers *an alert about the potential security issues* of existing AI generation systems.

2 Background

2.1 Diffusion Probabilistic Models

The framework of diffusion probabilistic models involves gradually diffusing the complex target data distribution to a simple noise distribution, such as white Gaussian, and solving the corresponding reverse process to generate new samples [12, 31]. Both the diffusion and denoising processes can

be characterized by temporally continuous stochastic differential equations (SDEs) [31]. From another perspective, Song et al. [31] derive deterministic processes (probability-flow ODEs) that are equivalent to the stochastic diffusion and denoising processes in the sense of marginal probability densities for all the time. In this work, we develop the AdjointDPM based on adjoint sensitivity methods from the ODE domain.

To be precise, let q_0 denote the unknown d -dimensional data distribution. Song et al. [31] formulated the forward diffusion process $\{\mathbf{x}(t)\}_{t \in [0, T]}$ as follows

$$d\mathbf{x}_t = f(t)\mathbf{x}_t dt + g(t) d\mathbf{w}_t, \quad \mathbf{x}_0 \sim q_0(\mathbf{x}), \quad t \in [0, T], \quad (2)$$

where \mathbf{x}_t is the state at time t , \mathbf{w}_t is the standard Wiener process (Brownian motion), $f(t)\mathbf{x}_t$ is a vector-valued function called the *drift* coefficient of \mathbf{x}_t , and $g(t)$ is a scalar function known as *diffusion* coefficient of \mathbf{x}_t . For the forward diffusion process, it is common to adopt the conditional probability as $q_{0t}(\mathbf{x}_t|\mathbf{x}_0) = \mathcal{N}(\mathbf{x}_t|\alpha_t\mathbf{x}_0, \sigma_t^2\mathbf{I})$ and the marginal distribution of \mathbf{x}_T to be approximately $\mathcal{N}(0, \sigma_T^2\mathbf{I})$. Then starting from samples $\mathbf{x}_T \sim \mathcal{N}(0, \sigma_T^2\mathbf{I})$, under some regularity conditions, we have a reverse process corresponding to the forward process as

$$d\mathbf{x}_t = [f(t)\mathbf{x}_t - g(t)^2 \nabla_{\mathbf{x}_t} \log q_t(\mathbf{x}_t)] dt + g(t) d\mathbf{w}_t, \quad \mathbf{x}_T \sim \mathcal{N}(0, \sigma_T^2\mathbf{I}), \quad t \in [0, T]. \quad (3)$$

In Eqn. (3), there is an unknown term $\nabla_{\mathbf{x}} \log q_t(\mathbf{x})$, which is known as the *score function*. We can estimate the score function by training a neural network $\epsilon_\theta(\mathbf{x}_t, t)$ for matching $\epsilon_\theta(\mathbf{x}_t, t)$ and $-\sigma_t \nabla_{\mathbf{x}} \log q_t(\mathbf{x}_t)$ with the objective function as follows:

$$\mathcal{L}_{\text{SM}}(\theta) := \mathbb{E}_t \left\{ \lambda(t) \mathbb{E}_{\mathbf{x}_0} \mathbb{E}_{\epsilon} [\|\epsilon_\theta(\mathbf{x}_t, t) - \epsilon\|_2^2] \right\}, \quad (4)$$

where $\lambda(\cdot) > 0$ is a weighting function, $\epsilon \sim \mathcal{N}(\epsilon|0, \mathbf{I})$, and $\mathbf{x}_t = \alpha_t\mathbf{x}_0 + \sigma_t\epsilon$.

As shown in [31], there exists a corresponding deterministic process whose trajectory shares the same set of marginal probability densities $\{q_t(\mathbf{x})\}_{t=0}^T$ as the SDE (3), and the form of the ODE is

$$d\mathbf{x} = \left[f(t)\mathbf{x}_t - \frac{1}{2}g(t)^2 \nabla_{\mathbf{x}} \log q_t(\mathbf{x}) \right] dt. \quad (5)$$

Thus, we can use the well-trained neural network $\epsilon_\theta(\mathbf{x}_t, t)$ to generate new samples by solving Eqn. (6) from T to 0 with initial sample \mathbf{x}_T drawn from $\mathcal{N}(0, \sigma_T^2\mathbf{I})$.

$$d\mathbf{x} = \left[f(t)\mathbf{x}_t + \frac{g(t)^2}{2\sigma_t} \epsilon_\theta(\mathbf{x}_t, t) \right] dt \quad (6)$$

For conditional sampling, classifier-free guidance (CFG) [11] has been widely used in various tasks for improving the sample quality, including text-to-image, image-to-image, class-to-image generation [28, 5, 22]. During training, one may simultaneously train unconditional and conditional prediction models with the same parameterized model $\epsilon_\theta(\mathbf{x}_t, t, c)$. The unconditional mode is triggered by setting c to be a fixed special placeholder \emptyset . Hence, the sampling model becomes

$$\tilde{\epsilon}_\theta(\mathbf{x}_t, t, c) := s \cdot \epsilon_\theta(\mathbf{x}_t, t, c) + (1 - s) \cdot \epsilon_\theta(\mathbf{x}_t, t, \emptyset),$$

and we can generate new samples with conditional variables by solving Eqn. (6) and replacing $\epsilon_\theta(\mathbf{x}_t, t)$ with $\tilde{\epsilon}_\theta(\mathbf{x}_t, t, c)$.

This paper mainly focuses on the optimization problem based on the generated samples of DPMs solved by probability-flow ODEs. Denote the generation mapping of a probability-flow ODE as Φ and our generated samples as

$$\mathbf{x}_0 = \Phi(\mathbf{x}_T, c, \epsilon_\theta) = \mathbf{x}_T + \int_T^0 \left[f(t)\mathbf{x}_t + \frac{g(t)^2}{2\sigma_t} \tilde{\epsilon}_\theta(\mathbf{x}_t, t, c) \right] dt,$$

i.e., the output samples are determined by the initial sample \mathbf{x}_T , the conditional variable c , and the noise prediction models ϵ_θ . Thus, if we want to customize the generated contents based on a loss function on \mathbf{x}_0 , we have three options—tuning the initial noise \mathbf{x}_T , the conditional variable c , or the weights θ by backpropagating the loss.

2.2 Adjoint Sensitivity Methods

To efficiently obtain the gradients of the loss function L with respect to ψ , we leverage the family of *adjoint sensitivity methods* in the study of Neural ODEs [3] to solve Eqn. (1). For simplicity, we denote $\mathbf{s}(\mathbf{x}_t, t, \theta, c) = f(t)\mathbf{x}_t + \frac{g(t)^2}{2\sigma_t}\tilde{\epsilon}_\theta(\mathbf{x}_t, t, c)$, and our objective function becomes

$$L(\mathbf{x}_0) = L\left(\mathbf{x}_T + \int_T^0 \mathbf{s}(\mathbf{x}_t, t, \theta, c) dt\right).$$

To optimize L , we need to compute the gradients with respect to its parameters $\{\mathbf{x}_T, t, \theta, c\}$. First consider $\frac{\partial L}{\partial \mathbf{x}_T}$. We introduce the adjoint state $\mathbf{a}(t) = \frac{\partial L}{\partial \mathbf{x}_t}$, which represents how the loss depends on the state \mathbf{x}_t at any time t . The dynamics of $\mathbf{a}(t)$ are given by another ODE,

$$\frac{d\mathbf{a}(t)}{dt} = -\mathbf{a}(t)^T \frac{\partial \mathbf{s}(\mathbf{x}_t, t, \theta, c)}{\partial \mathbf{x}_t}, \quad (7)$$

which can be thought of as the instantaneous analog of the chain rule. Since $\frac{\partial L}{\partial \mathbf{x}_0}$ is known, we can compute $\frac{\partial L}{\partial \mathbf{x}_T}$ by solving the initial value problem (IVP) backwards in time T to 0 of ODE in (7).

Similarly, for t and θ , we can regard them as if they were part of the augmented state

$$\frac{d}{dt} [\mathbf{x}, \theta, t] (t) := [\mathbf{s}(\mathbf{x}_t, t, \theta, c), 0, 1].$$

Noted that we omit the parameter c here because both c and θ serve as the *control* of the dynamics and have the same functionality in the ODE. One can use the following method to compute $\frac{\partial L}{\partial c}$ by simply replacing θ to c .

The corresponding adjoint state to this augmented state are

$$\mathbf{a}_{\text{aug}}(t) := [\mathbf{a}(t), \mathbf{a}_\theta(t), \mathbf{a}_t(t)], \quad \mathbf{a}_\theta := \frac{\partial L}{\partial \theta}, \quad \text{and} \quad \mathbf{a}_t := \frac{\partial L}{\partial t}.$$

In addition, \mathbf{a}_{aug} is governed by:

$$\frac{d\mathbf{a}_{\text{aug}}}{dt} = -[\mathbf{a} \frac{\partial \mathbf{s}}{\partial \mathbf{x}}, \mathbf{a} \frac{\partial \mathbf{s}}{\partial \theta}, \mathbf{a} \frac{\partial \mathbf{s}}{\partial t}]. \quad (8)$$

By solving the IVP from time T to 0 of Eqn. (8), we obtain the gradients of L w.r.t. $\{\mathbf{x}_t, \theta, t\}$. The explicit algorithm [3] is shown in Algorithm 1.

Algorithm 1 Reverse-mode derivative of an ODE initial value problem

Input: Dynamics parameter θ , start time t_0 , end time t_1 , final state \mathbf{x}_{t_1} , loss gradient $\partial L / \partial \mathbf{x}_{t_1}$.

$a(t_1) = \frac{\partial L}{\partial \mathbf{x}_{t_1}}, a_\theta(t_1) = \mathbf{0}, z_0 = [\mathbf{x}_{t_1}, a(t_1), a_\theta(t_1)]$ ▷ Define initial augmented state.

def AugDynamics($[\mathbf{x}_t, \mathbf{a}_t, \cdot], t, \theta$) ▷ Define dynamics on augmented state.

return $[\mathbf{s}(\mathbf{x}_t, t, \theta, c), -\mathbf{a}_t^T \frac{\partial \mathbf{s}}{\partial \mathbf{x}}, -\mathbf{a}_t^T \frac{\partial \mathbf{s}}{\partial \theta}]$ ▷ Concatenate time-derivatives

$[\mathbf{x}_{t_0}, \frac{\partial L}{\partial \mathbf{x}_{t_0}}, \frac{\partial L}{\partial \theta}] = \text{ODESolve}(z_0, \text{AugDynamics}, t_1, t_0, \theta)$ ▷ Solve reverse-time ODE

Return: $[\frac{\partial L}{\partial \mathbf{x}_{t_0}}, \frac{\partial L}{\partial \theta}]$ ▷ Return gradients

2.3 Text-to-Image Customization

Text-to-image customization aims to personalize a generative model for synthesizing new images of a specific target property. Existing customization methods typically tackle this task by either representing the property via a text embedding [7, 20, 33] or finetuning the weights of the generative model [27, 15, 10]. For example, Textual-Inversion [7] inverts the common identity shared by several images into a unique textual embedding. To make the learned embedding more expressive, Daras and Dimakis [4] and Voynov et al. [32] generalize the unique embedding to depend on the diffusion time or the layer index of the denoising UNet, respectively. In the other line, DreamBooth [27] learns a unique identifier placeholder and finetunes the whole diffusion model for identity customization. To

speed up and alleviate the overfitting, Custom Diffusion [16] and SVDiff [10] only update a small subset of weights. Most of these existing methods assume that a handful of image examples (at least 3-5 examples) sharing the same concept or property are provided by the user in the first place. They are thus not suitable for cases wherein the concept only can be described by an abstract metric (*e.g.*, adversarial) or only one or two examples are available. In contrast, this paper relaxes the requirement of data samples and proposes the AdjointDPM for model customization only under the supervision of a differentiable loss.

3 Improvements of Adjoint Sensitivity Methods on Diffusion Models

In this section, we apply adjoint sensitivity methods for gradient backpropagation in diffusion models. When we optimize the model’s parameters \mathbf{x}_T or θ (including the conditioning c), we need first to generate new samples via the forward ODE (6) and then to solve the backward adjoint ODE (8) to compute the gradients of loss with respect to the parameters. One can apply general-purpose numerical ODE solvers, such as Euler–Maruyama and Runge–Kutta methods [1], for solving the ODE. Here, we attempt to improve the efficiency of the vanilla adjoint sensitivity methods by exploiting the semi-linear structure of the diffusion ODE functions (6), which has been used in several existing works for accelerating DPM samplers [18, 19, 14, 35].

3.1 Exponential Integration and Reparameterization

We first rewrite the reverse ODE function in Algorithm 1 as:

$$\mathbf{d} \begin{bmatrix} \mathbf{x}_t \\ \frac{\partial L}{\partial \mathbf{x}_t} \\ \frac{\partial L}{\partial \theta} \\ \frac{\partial L}{\partial t} \end{bmatrix} = - \begin{bmatrix} -f(t)\mathbf{x}_t - \frac{g(t)^2}{2\sigma_t} \tilde{\epsilon}_\theta(\mathbf{x}_t, t, c) \\ f(t) \frac{\partial L}{\partial \mathbf{x}_t} + \frac{\partial L}{\partial \mathbf{x}_t} \frac{g(t)^2}{2\sigma_t} \frac{\partial \tilde{\epsilon}_\theta(\mathbf{x}_t, t, c)}{\partial \mathbf{x}_t} \\ \frac{\partial L}{\partial \mathbf{x}_t} \frac{g(t)^2}{2\sigma_t} \frac{\partial \tilde{\epsilon}_\theta(\mathbf{x}_t, t, c)}{\partial \theta} \\ \frac{df(t)}{dt} \frac{\partial L}{\partial \mathbf{x}_t} \mathbf{x}_t + \frac{\partial L}{\partial \mathbf{x}_t} \frac{\partial [g(t)^2/2\sigma_t \tilde{\epsilon}_\theta(\mathbf{x}_t, t, c)]}{\partial t} \end{bmatrix} dt, \quad (9)$$

and observe the ODEs governing \mathbf{x}_t and $\frac{\partial L}{\partial \mathbf{x}_t}$ both contain linear and nonlinear parts. If we directly use off-the-shelf numerical solvers on Eqn. (9), it causes discretization errors of both the linear and nonlinear terms.

To avoid this, we use the *exponential integration* to transform the ODE (6) into a simple non-stiff ODE. We multiply an integrating factor $\exp(-\int_0^t f(\tau)d\tau)$ on both sides of Eqn. (6) and obtain

$$\frac{de^{-\int_0^t f(\tau)d\tau} \mathbf{x}_t}{dt} = e^{-\int_0^t f(\tau)d\tau} \frac{g(t)^2}{2\sigma_t} \tilde{\epsilon}_\theta(\mathbf{x}_t, t, c).$$

Denote $\mathbf{y}_t = e^{-\int_0^t f(\tau)d\tau} \mathbf{x}_t$, then we have

$$\frac{d\mathbf{y}_t}{dt} = e^{-\int_0^t f(\tau)d\tau} \frac{g(t)^2}{2\sigma_t} \tilde{\epsilon}_\theta \left(e^{\int_0^t f(\tau)d\tau} \mathbf{y}_t, t, c \right). \quad (10)$$

We also denote $\frac{d\rho}{dt} = e^{-\int_0^t f(\tau)d\tau} \frac{g(t)^2}{2\sigma_t}$ and $\rho = \gamma(t)$. In diffusion models, the choice of $e^{-\int_0^t f(\tau)d\tau} \frac{g(t)^2}{2\sigma_t}$ is usually a monotone function with respect to t . For example, when we choose $f(t) = \frac{d \log \alpha}{dt}$ and $g^2(t) = \frac{d\sigma_t^2}{dt} - 2 \frac{d \log \alpha}{dt} \sigma_t^2$ in VP-SDE [31], we have $\gamma(t) = \alpha_0 \frac{\sigma_t}{\alpha_t} - \sigma_0$, which monotonically increases when t increases from 0 to T . Thus, a bijective mapping exists between ρ and t , and we can reparameterize (10) as:

$$\frac{d\mathbf{y}}{d\rho} = \tilde{\epsilon}_\theta \left(e^{\int_0^{\gamma^{-1}(\rho)} f(\tau)d\tau} \mathbf{y}, \gamma^{-1}(\rho), c \right). \quad (11)$$

We also reparameterize the reverse ODE function in Algorithm 1 as follows

$$\mathbf{d} \begin{bmatrix} \mathbf{y} \\ \frac{\partial L}{\partial \mathbf{y}} \\ \frac{\partial L}{\partial \theta} \\ \frac{\partial L}{\partial \rho} \end{bmatrix} = - \begin{bmatrix} -\tilde{\epsilon}_\theta \left(e^{\int_0^{\gamma^{-1}(\rho)} f(\tau)d\tau} \mathbf{y}, \gamma^{-1}(\rho), c \right) \\ \frac{\partial L}{\partial \mathbf{y}} \frac{\partial \tilde{\epsilon}_\theta \left(e^{\int_0^{\gamma^{-1}(\rho)} f(\tau)d\tau} \mathbf{y}, \gamma^{-1}(\rho), c \right)}{\partial \mathbf{y}} \\ \frac{\partial L}{\partial \mathbf{y}} \frac{\partial \tilde{\epsilon}_\theta \left(e^{\int_0^{\gamma^{-1}(\rho)} f(\tau)d\tau} \mathbf{y}, \gamma^{-1}(\rho), c \right)}{\partial \theta} \\ \frac{\partial L}{\partial \mathbf{y}} \frac{\partial \tilde{\epsilon}_\theta \left(e^{\int_0^{\gamma^{-1}(\rho)} f(\tau)d\tau} \mathbf{y}, \gamma^{-1}(\rho), c \right)}{\partial \rho} \end{bmatrix} d\rho. \quad (12)$$

Now instead of solving Eqn. (6) and Eqn. (9), we use off-the-shelf numerical ODE solvers to solve Eqn. (11) and Eqn. (12), and term this method AdjointDPM.

3.2 Error Control

Here, we first show that the exact solutions of the reparameterized ODEs are equivalent to the original ones. For the equation in the first row of Eqn. (12), its exact solution is:

$$\mathbf{y}_{\rho(t)} = \mathbf{y}_{\rho(s)} + \int_{\rho(s)}^{\rho(t)} \tilde{\epsilon}_{\theta} \left(e^{\int_0^{\gamma^{-1}(\rho)} f(\tau) d\tau} \mathbf{y}, \gamma^{-1}(\rho), c \right) d\rho. \quad (13)$$

We can rewrite it as:

$$\begin{aligned} e^{-\int_0^t f(\tau) d\tau} \mathbf{x}_t &= e^{-\int_0^s f(\tau) d\tau} \mathbf{x}_s + \int_s^t \frac{d\rho}{d\tau} \tilde{\epsilon}_{\theta}(\mathbf{x}_{\tau}, \tau, c) d\tau \\ \Rightarrow \mathbf{x}_t &= e^{\int_s^t f(\tau) d\tau} \mathbf{x}_s + \int_s^t e^{\int_{\tau}^t f(r) dr} \frac{g(\tau)^2}{2\sigma_{\tau}} \tilde{\epsilon}_{\theta}(\mathbf{x}_{\tau}, \tau, c) d\tau, \end{aligned}$$

which is equivalent to the exact solution of the equation in the first row of Eqn. (9). Similarly, for the second equation in (12), its exact solution is

$$\begin{aligned} \frac{\partial L}{\partial \mathbf{y}_{\rho(t)}} &= \frac{\partial L}{\partial \mathbf{y}_{\rho(s)}} - \int_{\rho(s)}^{\rho(t)} \frac{\partial L}{\partial \mathbf{y}_{\rho}} \frac{\partial \tilde{\epsilon}_{\theta} \left(e^{\int_0^{\gamma^{-1}(\rho)} f(\tau) d\tau} \mathbf{y}, \gamma^{-1}(\rho), c \right)}{\partial \mathbf{y}_{\rho}} d\rho \\ \Rightarrow \frac{\partial L}{\partial \mathbf{x}_t} &= e^{\int_t^s f(\tau) d\tau} \frac{\partial L}{\partial \mathbf{x}_s} - \int_s^t \frac{\partial L}{\partial \mathbf{x}_{\tau}} e^{\int_t^{\tau} f(r) dr} \frac{g(\tau)^2}{2\sigma_{\tau}} \frac{\partial \tilde{\epsilon}_{\theta}(\mathbf{x}_{\tau}, \tau, c)}{\partial \mathbf{x}_{\tau}} d\tau, \end{aligned} \quad (14)$$

which is also equivalent to the solution of the second equation in (9). Thus, when we numerically solve non-stiff ODEs in Eqns (11) and (12), there are only discretization errors for nonlinear functions and the closed form of integration of linear parts have been solved exactly without any numerical approximation.

In summary, we reformulate the forward and reverse ODE functions in this section and show that by using off-the-shelf numerical ODE solvers on reparameterized ODEs, the discretization error of the linear part will not be introduced by AdjointDPM. In Section 3.3, we experimentally compare the FID of generated images by solving Eqn. (6) and Eqn. (11) with the same number of network function evaluations (NFE). The results verify the superiority of solving Eqn. (11) regarding error control.

3.3 Performance of AdjointDPM

As we need to solve two ODEs (forward one to generate images and reverse one to obtain the gradients), we should trade-off between the sample quality and solving time. We choose a suitable NFE number for ODE solvers so that the DPM generates content with good quality while does not take too much time. Thus, we compare the performance of AdjointDPM (solving the reparameterized ODEs) to the case of solving the original ones under small NFE regions (≤ 50).

Table 1: FID values for VPSDE models evaluated on CIFAR10 in small NFE regions.

NFE	Solving (6)	Solving (11)
10	9.50	4.36
20	8.27	2.90
50	5.64	2.58

We follow the implementation of DPM in [31] and use the publicly released checkpoints³ (trained on the CIFAR10 dataset) to generate images in an unconditional manner. We use the *torchdiffeq* package⁴, and solve Eqn. (6) and Eqn. (11) via the Adams–Bashforth numerical solver with order 4 in *torchdiffeq*.

We generate the same number of images as the training set and compute the FID between the generated images and the real ones. Table 1 shows the FID evaluations of solving different ODEs in continuous-time VPSDE models

on CIFAR10. From Table 1, we observe that, after reparameterizing the forward generation process to a non-stiff ODE function, we can generate higher-quality samples with lower FID under the same NFEs.

³https://github.com/yang-song/score_sde

⁴<https://github.com/rtqichen/torchdiffeq>

4 Applications

In this section, we apply AdjointDPM to perform three interesting tasks. The first two tasks aim to optimize the parameters of DPMs to generate images of certain customized properties, *i.e.*, converting visual effects into optimized prompt embeddings (Section 4.1) and finetuning network weights for stylization (Section 4.2). The third task aims to audit the security of DPM generation systems by crafting adversarial samples which can bypass a classifier filter (*e.g.*, NSFW) but still appear visually harmful (Section 4.3). The experimental results demonstrate that our method can effectively back-propagate the loss information on the generated images to the related variables of DPMs.

4.1 Text Embedding Inversion

Our first application concerns using AdjointDPM to convert visual effects (*e.g.*, bokeh and relighting) into an identification text embedding $\#$. After optimization, we can combine the obtained embedding with various text prompts to generate images with the same visual effect. Suppose we are provided a text-to-image DPM $\Phi(\mathbf{x}_T, c, \epsilon_\theta)$, we can generate an image \mathbf{x} by denoising randomly sampled noise \mathbf{x}_T under the guidance of the prompt c . The generated image \mathbf{x} can be further edited by a professional photographer to improve the aesthetic quality (*e.g.*, color, tone, and bokeh). We want to distill the editing effect in the edited image \mathbf{x}^* into a special embedding $\#$. We use \mathbf{x}^* or its feature as a reference to define a loss $L(\cdot)$ that measures the distance to the target effect, such as the ℓ_2 or perceptual loss. The special embedding $\#$ can be obtained by solving the following optimization problem:

$$\min_{\#} L(\mathbf{x}^*, \Phi(\mathbf{x}_T, \{c, \#\}, \epsilon_\theta)).$$

We utilize the publicly released Stable Diffusion⁵ models [26] for image generation and set the loss function as the mean squared error (MSE) between the target images and the generated images. We aim to optimize a prompt embedding in the CLIP [23] embedding space and use the obtained embedding for image generation by concatenating it with the embeddings of other text prompts.

We first generate an image with a text prompt c and randomly sampled noise \mathbf{x}_T . To improve the visual quality of the generated image, we either manually edit it by adjusting the color and tone or concatenate the prompt c with an effect token c^* and generate another image \mathbf{x}^* on the condition of $\{c, c^*\}$. We optimize the special embedding $\#$ to recover the editing effect. As shown in Fig. 1, we observe AdjointDPM successfully yields an embedding $\#$ that can ensure the appearance of target visual effects, including the *bokeh* and *relighting*. Furthermore, the obtained embeddings $\#$ also generalize well to other starting noise and other text prompts. For example, the bokeh- $\#$ is optimized on a pair of *totoro* images; it also can be used for generating different images of *totoro* and other objects like *dog*. Similarly, the obtained $\#$ corresponding to manual editing (“converting to black and white”) also can be used for novel scene generation. More examples are shown in Appendix A.1.

4.2 Stylization

In the second application, we consider finetuning the parameters of the denoising UNet for stylization by using AdjointDPM. The target style is defined by given Gram matrices [8], which are computed based on the features (extracted from a pretrained VGG [8] model⁶) of a stylized image. Here we denote the features extracted from the VGG as \mathbf{F} and the gram matrix $\mathbf{G} = \mathbf{F}\mathbf{F}^T$. We can sample multiple noise-prompt pairs to generate images, $\{(\mathbf{x}_T^i, c^i)\}_{i=1}^N$, for training. We fine-tune the parameters of UNet by optimizing the combination of style loss L_s and content loss L_c , which is defined as follows:

$$\min_{\theta} \frac{1}{N} \sum_i [w_s L_s(\mathbf{G}_{\text{style}}, \mathbf{G}(\Phi(\mathbf{x}_T^i, c^i, \epsilon_\theta))) + w_c L_c(\mathbf{F}_{\text{initial}}, \mathbf{F}(\Phi(\mathbf{x}_T^i, c^i, \epsilon_\theta)))] ,$$

where w_s and w_c are the weights for style loss and content loss respectively, $\mathbf{G}_{\text{style}}$ are the Gram matrices of target style image and $\mathbf{F}_{\text{initial}}$ are the features of the generated image before parameter tuning. We use mean squared errors (MSE) for style loss L_s and content loss L_c .

⁵<https://github.com/huggingface/diffusers>

⁶https://pytorch.org/tutorials/advanced/neural_style_tutorial.html

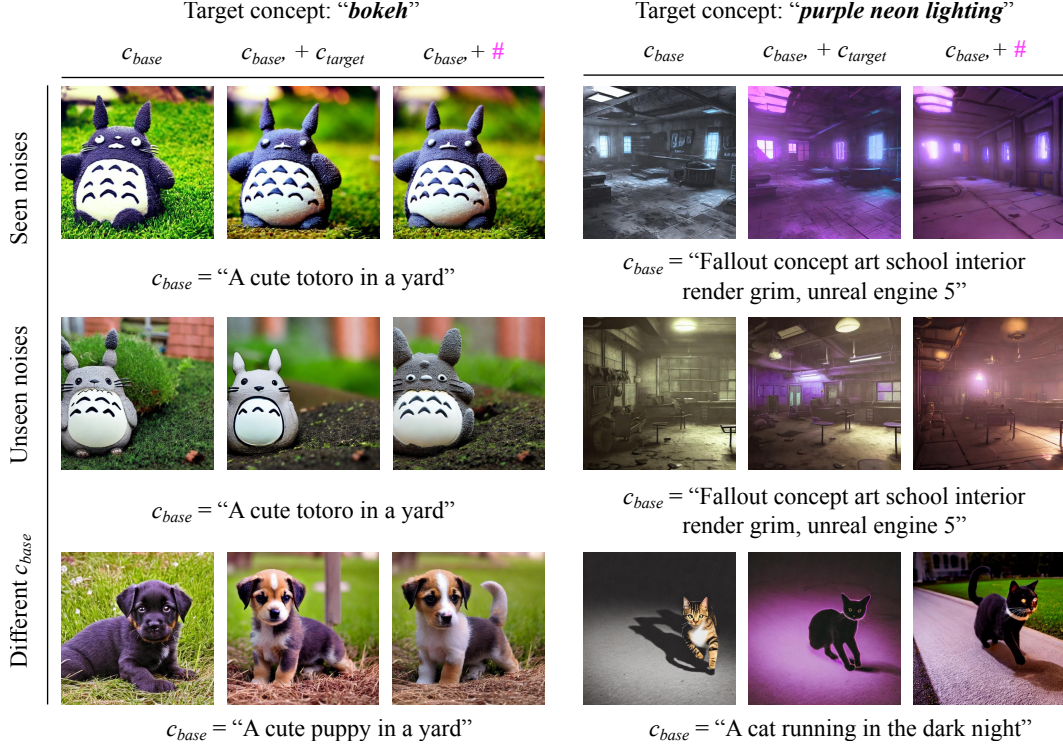


Figure 1: Examples on text embedding inversion



Figure 2: Stylization examples

Specifically, we still use the Stable Diffusion model for image generation. We construct 10 prompts corresponding to ten of the CIFAR100 classes and generate 100 images (10 images for each prompt) to compose our training dataset. As shown in the left part of Fig. 2, the finetuned DPM can generate stylized images of different objects after finetuning. Besides, we can also observe the stylization even on not seen objects and noises during optimization (shown in the right part of Fig. 2). More details and examples on stylization are shown in Appendix A.2.

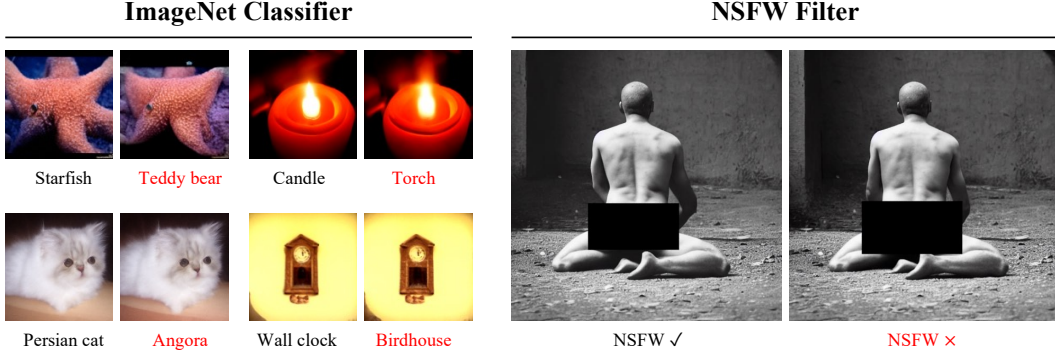


Figure 3: Left: Adversarial samples against an Imagenet classifier. We show the originally generated images with their class names on the left; these images are correctly classified. On the right, we show the corresponding adversarial images which successfully mislead the classifier. Right: Adversarial samples against the NSFW filter. We show the image generated by conditioning on the prompt “A photograph of a naked man” on the left. This image will be blocked by the NSFW filter. However, the right adversarial image circumvents the NSFW filter (Black squares are added by authors for publication).

4.3 Security Auditing

The last application concerns using AdjointDPM for auditing the security of AI generation systems. DPM-based image generation models have been widely-used in content creation platforms. The powerful DPMs are usually trained on large-scale datasets, such as LAION [30], which may contain unexpected and harmful data (*e.g.*, violence, discrimination, pornography, *etc.*). To avoid generating NSFW content, AI generation systems are usually equipped with an NSFW filter which blocks the outputs of potentially harmful content. However, deep neural networks have been shown to be vulnerable against adversarial examples in various understanding tasks [9, 34], including classification, detection, *etc.* This naturally raises the question—may existing DPMs generate content that can sneakily bypass the NSFW filter while still appearing visually NSFW?

Denote the content moderation filter as $f(\cdot)$. If the conditioning text c contains harmful concepts, the generated images of $\Phi(\mathbf{x}_T, c, \epsilon_\theta)$ will be filtered out by $f(\cdot)$. Here, the starting noise \mathbf{x}_T is randomly drawn from the normal distribution. We audit the security of $\Phi(\mathbf{x}_T, c, \epsilon_\theta)$ by optimizing a small adversarial perturbation δ on \mathbf{x}_T , such that $\Phi(\mathbf{x}_T + \delta, c, \epsilon_\theta)$ will mislead the filter $f(\cdot)$:

$$\max_{\delta: \|\delta\|_\infty \leq \tau} L(y, f(\Phi(\mathbf{x}_T + \delta, c, \epsilon_\theta))),$$

where y represents the label of “harmful” class and $L(\cdot, \cdot)$ measures the distance between y and the prediction of $f(\cdot)$, *e.g.*, the cross-entropy or the embedding similarity. The perturbation δ is restricted to have a small norm, *i.e.*, $\|\delta\|_\infty \leq \tau$, as we want to ensure the newly generated image is visually similar to the original one.

We use AdjointDPM to attack the Stable Diffusion model equipped with an NSFW filter. Results in Fig. 3 show SD can synthesize visually harmful images that bypass the NSFW filter. This observation raises an alert about the security issues of AI generation systems. *Our research community has to develop more advanced mechanisms to ensure the isolation between NSFW content and users, especially teenagers.* Besides NSFW security, we also evaluate the capability of DPMs in generating adversarial images of common objects. We have a similar observation. DPMs also can generate images that mislead pre-trained ImageNet classifiers. More details about the experiments are shown in the Appendix A.3.

5 Conclusion

This paper proposes AdjointDPM, a novel and flexible method for generating the content of target concepts based on DPM. AdjointDPM only requires a well-defined, computable, and differentiable loss on the generated content. AdjointDPM first solves the probability-flow ODE to generate content. Then, it uses the adjoint sensitivity method to backpropagate the gradients of defined loss to related parameters of DPMs. This process only consumes a constant GPU memory. Beyond the applications

introduced in this paper, AdjointDPM can be extended to generate contents that meet a wide variety of requirements, provided that these requirements are appropriately defined. For instance, one could draw a binary object mask on a section of an image, then use this mask to guide the position and shape of the generated object. This adaptability suggests a broad scope for potential applications of AdjointDPM.

6 Broader Impact

This work aims to address the problem of synthesizing images of target concepts and properties with the only need of a computable metric, not necessarily requiring reference examples. The proposed method, AdjointDPM, has both positive and negative societal impacts depending on its applications and uses. On the positive side, AdjointDPM enables more flexible customization of pre-trained DPMs and only necessitates a manually defined metric or loss for the generated content. Additionally, AdjointDPM can be employed to assess the security of DPM-based AI generation systems. On the downside, there is a risk of malicious actors utilizing AdjointDPM to create NSFW content that could deceive and evade moderation mechanisms. This work provides a flexible and tailored generation approach while also highlighting the potential security issues associated with DPM-based generation systems.

References

- [1] K. Atkinson, W. Han, and D. E. Stewart. *Numerical solution of ordinary differential equations*. John Wiley & Sons, 2011.
- [2] A. Blattmann, R. Rombach, H. Ling, T. Dockhorn, S. W. Kim, S. Fidler, and K. Kreis. Align your Latents: High-Resolution Video Synthesis with Latent Diffusion Models, Apr. 2023. arXiv:2304.08818 [cs].
- [3] R. T. Q. Chen, Y. Rubanova, J. Bettencourt, and D. K. Duvenaud. Neural ordinary differential equations. In *Advances in Neural Information Processing Systems*, volume 31, 2018.
- [4] G. Daras and A. Dimakis. Multiresolution textual inversion. In *NeurIPS 2022 Workshop on Score-Based Methods*, 2022.
- [5] P. Dhariwal and A. Nichol. Diffusion models beat GANs on image synthesis. In *Advances in Neural Information Processing Systems*, volume 34, 2021.
- [6] Z. Fei, M. Fan, and J. Huang. Gradient-Free Textual Inversion, Apr. 2023. arXiv:2304.05818 [cs].
- [7] R. Gal, Y. Alaluf, Y. Atzmon, O. Patashnik, A. H. Bermano, G. Chechik, and D. Cohen-Or. An Image is Worth One Word: Personalizing Text-to-Image Generation using Textual Inversion, Aug. 2022. arXiv:2208.01618 [cs].
- [8] L. Gatys, A. Ecker, and M. Bethge. A neural algorithm of artistic style. *Nature Communications*, 2015.
- [9] I. J. Goodfellow, J. Shlens, and C. Szegedy. Explaining and harnessing adversarial examples. In *3rd International Conference on Learning Representations, ICLR, San Diego, CA, USA*, 2015.
- [10] L. Han, Y. Li, H. Zhang, P. Milanfar, D. Metaxas, and F. Yang. SVDiff: Compact Parameter Space for Diffusion Fine-Tuning, Apr. 2023. arXiv:2303.11305 [cs].
- [11] J. Ho and T. Salimans. Classifier-free diffusion guidance. In *NeurIPS 2021 Workshop on Deep Generative Models and Downstream Applications*, 2021.
- [12] J. Ho, A. Jain, and P. Abbeel. Denoising diffusion probabilistic models. In *Advances in Neural Information Processing Systems*, volume 33, 2020.
- [13] J. Ho, W. Chan, C. Saharia, J. Whang, R. Gao, A. Gritsenko, D. P. Kingma, B. Poole, M. Norouzi, D. J. Fleet, et al. Imagen video: High definition video generation with diffusion models. *arXiv preprint arXiv:2210.02303*, 2022.

- [14] T. Karras, M. Aittala, T. Aila, and S. Laine. Elucidating the design space of diffusion-based generative models. In *Advances in Neural Information Processing Systems*, 2022.
- [15] B. Kavar, S. Zada, O. Lang, O. Tov, H. Chang, T. Dekel, I. Mosseri, and M. Irani. Imagic: Text-Based Real Image Editing with Diffusion Models, Mar. 2023. arXiv:2210.09276 [cs].
- [16] N. Kumari, B. Zhang, R. Zhang, E. Shechtman, and J.-Y. Zhu. Multi-concept customization of text-to-image diffusion. *arXiv preprint arXiv:2212.04488*, 2022.
- [17] H. Liu, Z. Chen, Y. Yuan, X. Mei, X. Liu, D. Mandic, W. Wang, and M. D. Plumbley. AudioLDM: Text-to-Audio Generation with Latent Diffusion Models, Feb. 2023. arXiv:2301.12503 [cs, eess].
- [18] C. Lu, Y. Zhou, F. Bao, J. Chen, C. Li, and J. Zhu. DPM-Solver: A fast ODE solver for diffusion probabilistic model sampling in around 10 steps. In *Advances in Neural Information Processing Systems*, 2022.
- [19] C. Lu, Y. Zhou, F. Bao, J. Chen, C. Li, and J. Zhu. DPM-Solver++: Fast solver for guided sampling of diffusion probabilistic models. *arXiv preprint arXiv:2211.01095*, 2022.
- [20] R. Mokady, A. Hertz, K. Aberman, Y. Pritch, and D. Cohen-Or. Null-text Inversion for Editing Real Images using Guided Diffusion Models, Nov. 2022. arXiv:2211.09794 [cs].
- [21] E. Molad, E. Horwitz, D. Valevski, A. R. Acha, Y. Matias, Y. Pritch, Y. Leviathan, and Y. Hoshen. Dreamix: Video Diffusion Models are General Video Editors, Feb. 2023. arXiv:2302.01329 [cs].
- [22] A. Q. Nichol, P. Dhariwal, A. Ramesh, P. Shyam, P. Mishkin, B. McGrew, I. Sutskever, and M. Chen. GLIDE: Towards photorealistic image generation and editing with text-guided diffusion models. In *International Conference on Machine Learning*, pages 16784–16804. PMLR, 2022.
- [23] A. Radford, J. W. Kim, C. Hallacy, A. Ramesh, G. Goh, S. Agarwal, G. Sastry, A. Askell, P. Mishkin, J. Clark, G. Krueger, and I. Sutskever. Learning Transferable Visual Models From Natural Language Supervision. In *Proceedings of the 38th International Conference on Machine Learning*, pages 8748–8763. PMLR, July 2021. ISSN: 2640-3498.
- [24] A. Ramesh, P. Dhariwal, A. Nichol, C. Chu, and M. Chen. Hierarchical Text-Conditional Image Generation with CLIP Latents, Apr. 2022. arXiv:2204.06125 [cs].
- [25] J. Rando, D. Paleka, D. Lindner, L. Heim, and F. Tramèr. Red-teaming the stable diffusion safety filter. In *NeurIPS ML Safety Workshop*, 2022.
- [26] R. Rombach, A. Blattmann, D. Lorenz, P. Esser, and B. Ommer. High-resolution image synthesis with latent diffusion models. In *Proceedings of the IEEE/CVF Conference on Computer Vision and Pattern Recognition*, pages 10684–10695, 2022.
- [27] N. Ruiz, Y. Li, V. Jampani, Y. Pritch, M. Rubinstein, and K. Aberman. DreamBooth: Fine Tuning Text-to-Image Diffusion Models for Subject-Driven Generation. Technical report, Aug. 2022. arXiv:2208.12242 [cs].
- [28] C. Saharia, W. Chan, S. Saxena, L. Li, J. Whang, E. L. Denton, K. Ghasemipour, R. Gontijo Lopes, B. Karagol Ayan, T. Salimans, et al. Photorealistic text-to-image diffusion models with deep language understanding. In *Advances in Neural Information Processing Systems*, volume 35, 2022.
- [29] F. Schneider. ArchiSound: Audio Generation with Diffusion, Jan. 2023. arXiv:2301.13267 [cs, eess].
- [30] C. Schuhmann, R. Beaumont, R. Vencu, C. Gordon, R. Wightman, M. Cherti, T. Coombes, A. Katta, C. Mullis, M. Wortsman, P. Schramowski, S. Kundurthy, K. Crowson, L. Schmidt, R. Kaczmarczyk, and J. Jitsev. LAION-5B: An open large-scale dataset for training next generation image-text models, 2022.

- [31] Y. Song, J. Sohl-Dickstein, D. P. Kingma, A. Kumar, S. Ermon, and B. Poole. Score-based generative modeling through stochastic differential equations. In *International Conference on Learning Representations*, 2021.
- [32] A. Voynov, Q. Chu, D. Cohen-Or, and K. Aberman. P+: Extended Textual Conditioning in Text-to-Image Generation, Mar. 2023. arXiv:2303.09522 [cs].
- [33] Y. Wen, N. Jain, J. Kirchenbauer, M. Goldblum, J. Geiping, and T. Goldstein. Hard Prompts Made Easy: Gradient-Based Discrete Optimization for Prompt Tuning and Discovery, Feb. 2023. arXiv:2302.03668 [cs].
- [34] H. Yan, J. Du, V. Tan, and J. Feng. On robustness of neural ordinary differential equations. In *International Conference on Learning Representations*, 2020.
- [35] Q. Zhang and Y. Chen. Fast sampling of diffusion models with exponential integrator. In *NeurIPS Workshop on Score-Based Methods*, 2022.
- [36] D. Zhou, W. Wang, H. Yan, W. Lv, Y. Zhu, and J. Feng. MagicVideo: Efficient Video Generation With Latent Diffusion Models, Nov. 2022. arXiv:2211.11018 [cs].

Contents

1	Introduction	1
2	Background	2
2.1	Diffusion Probabilistic Models	2
2.2	Adjoint Sensitivity Methods	4
2.3	Text-to-Image Customization	4
3	Improvements of Adjoint Sensitivity Methods on Diffusion Models	5
3.1	Exponential Integration and Reparameterization	5
3.2	Error Control	6
3.3	Performance of AdjointDPM	6
4	Applications	7
4.1	Text Embedding Inversion	7
4.2	Stylization	7
4.3	Security Auditing	9
5	Conclusion	9
6	Broader Impact	10
A	Appendix	13
A.1	More Examples on Text Embedding Inversion	13
A.2	More Examples on Finetuning Weights for Stylization	14
A.2.1	Qualitative comparisons to Textual-Inversion and DreamBooth	14
A.3	Experimental Details and More Results on Security Auditing	15
A.4	Implementation of AdjointDPM on VP-SDE	19

A Appendix

A.1 More Examples on Text Embedding Inversion

To optimize a suitable text embedding for unknown concepts, we fix the text embedding of c_{base} and fine-tune the remaining text embedding for unknown concepts. Then we minimize the MSE loss between initially generated images and target images. We run 50 epochs with AdamW optimizer of learning rate 0.1. In addition to visual effects *bokeh* and *relighting* we show in Sec. 4.1, we can also obtain text embeddings for other visual effects such as *stylization*. We present more examples of text embedding inversion in Fig. 4.

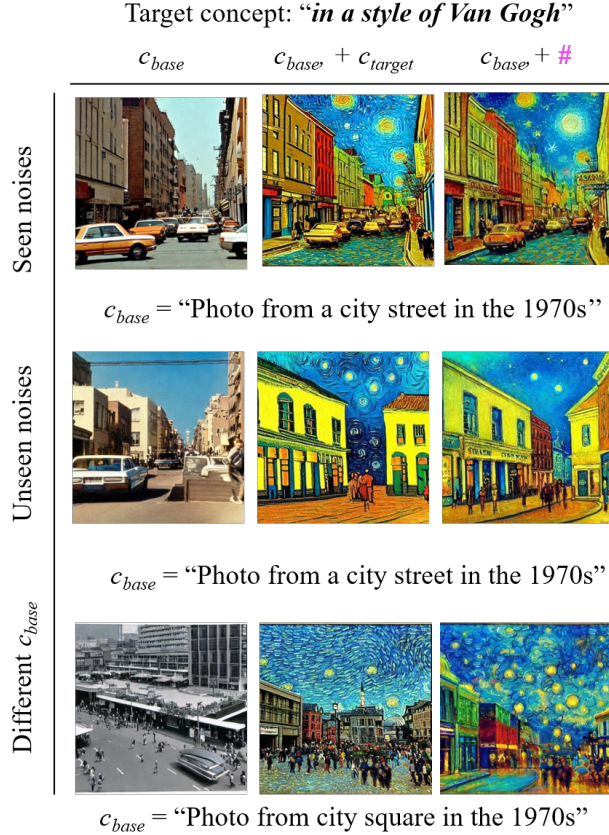


Figure 4: Examples on text embedding inversion

A.2 More Examples on Finetuning Weights for Stylization

In this section, we introduce the experimental details of stylization and present more stylized examples on seen noises and seen classes, unseen noises and seen classes, and unseen noises and unseen classes.

For training, we choose ten classes from CIFAR-100 classes, which are [“An airplane”, “A cat”, “A truck”, “A forest”, “A house”, “sunflowers”, “A bottle”, “A bed”, “Apples”, “A clock”]. Then we randomly generate 10 samples from each class to compose our training dataset. Besides, we directly use these class names as the input prompt to Stable Diffusion⁷. We optimize the parameters of cross attention layers of UNet for 8 epochs by using AdamW optimizer with learning rate 10^{-4} . We show more stylization results on 100 training samples (seen noises and seen classes) in Fig. 5. Meanwhile, we also show more examples of seen classes and unseen noises in Fig. 6 and examples of unseen classes and unseen noises in Fig. 7. In Fig. 8, we also show the stylization results on other target style images, in which one is downloaded from the showcase set of Midjourney⁸ and the other is the Starry Night by Van Gogh.

A.2.1 Qualitative comparisons to Textual-Inversion and DreamBooth

We also provide visual comparisons to Textual Inversion [7] and DreamBooth [27] in Fig. 9. We follow the implementation of Textual Inversion⁹ and DreamBooth¹⁰. For textual inversion, we use the same target style image in Sec. 4.2 as the training dataset. As in our AdjointDPM model, we use one style image for training, for fair comparison, the training dataset to Textual Inversion and

⁷<https://github.com/CompVis/stable-diffusion>

⁸https://cdn.midjourney.com/61b8bd5d-846b-4f69-bdc1-0ae2a2abcce8/grid_0.webp

⁹https://huggingface.co/docs/diffusers/training/text_inversion

¹⁰<https://huggingface.co/docs/diffusers/training/dreambooth>



Figure 5: Stylization examples on seen classes and seen noises

DreamBooth also include only one style image. We set the *learnable property* as “style”, *placeholder token* as “<bengiles>”, *initializer token* as “flowers” in Textual Inversion. Then we run 5000 epochs with a learning rate 5×10^{-4} to train the Textual Inversion. For DreamBooth, we set *instance prompt* as “bengiles flowers”. Then we run 1000 epochs with a learning rate 1×10^{-6} to train the DreamBooth. In Fig. 9, we show the stylization examples generated by using Textual Inversion and DreamBooth. We can observe distinct differences in the stylization outcomes when comparing the Textual Inversion and DreamBooth approaches to our AdjointDPM methods. In some cases, for Textual Inversion and DreamBooth, we have noticed that the main objects within an image can vanish, resulting in the entire image being predominantly occupied by the applied “style.”

A.3 Experimental Details and More Results on Security Auditing

In this section, we provide explicit details about generating adversarial examples against an ImageNet classifier and the NSFW filter in Stable Diffusion, respectively.

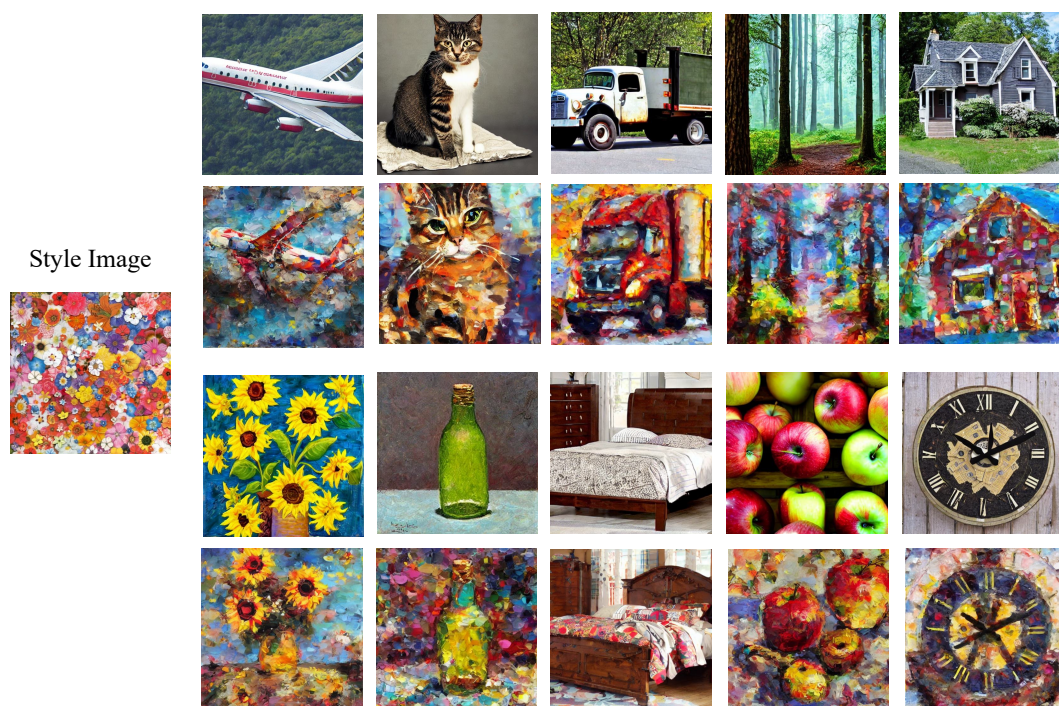


Figure 6: Stylization examples on seen classes and unseen noises

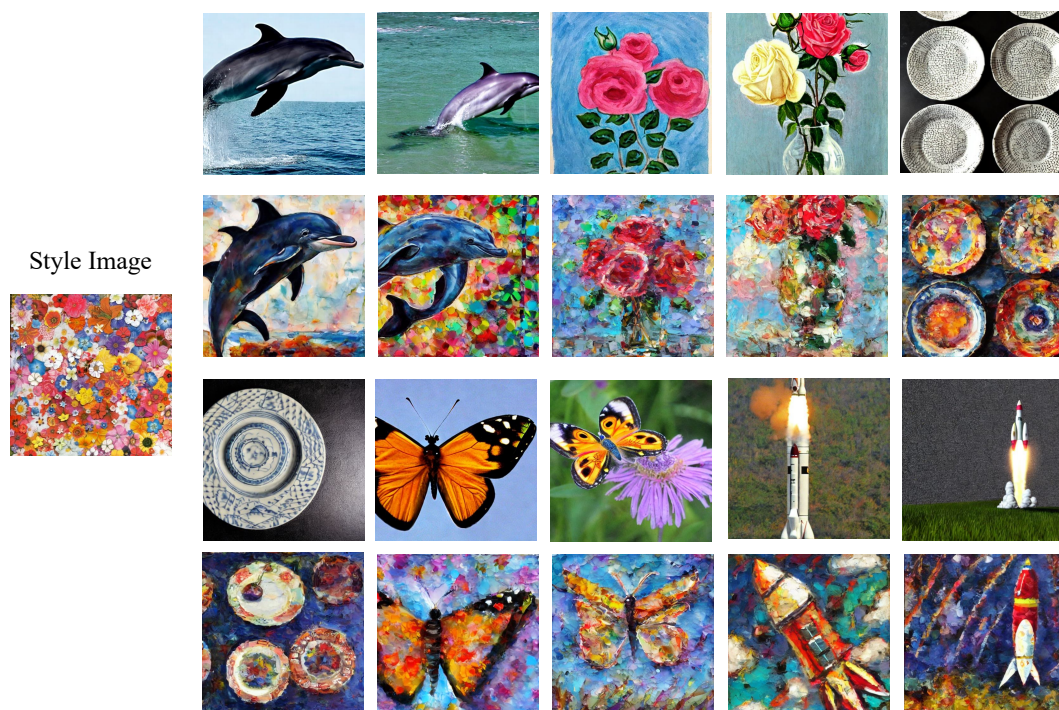


Figure 7: Stylization examples on unseen classes and unseen noises

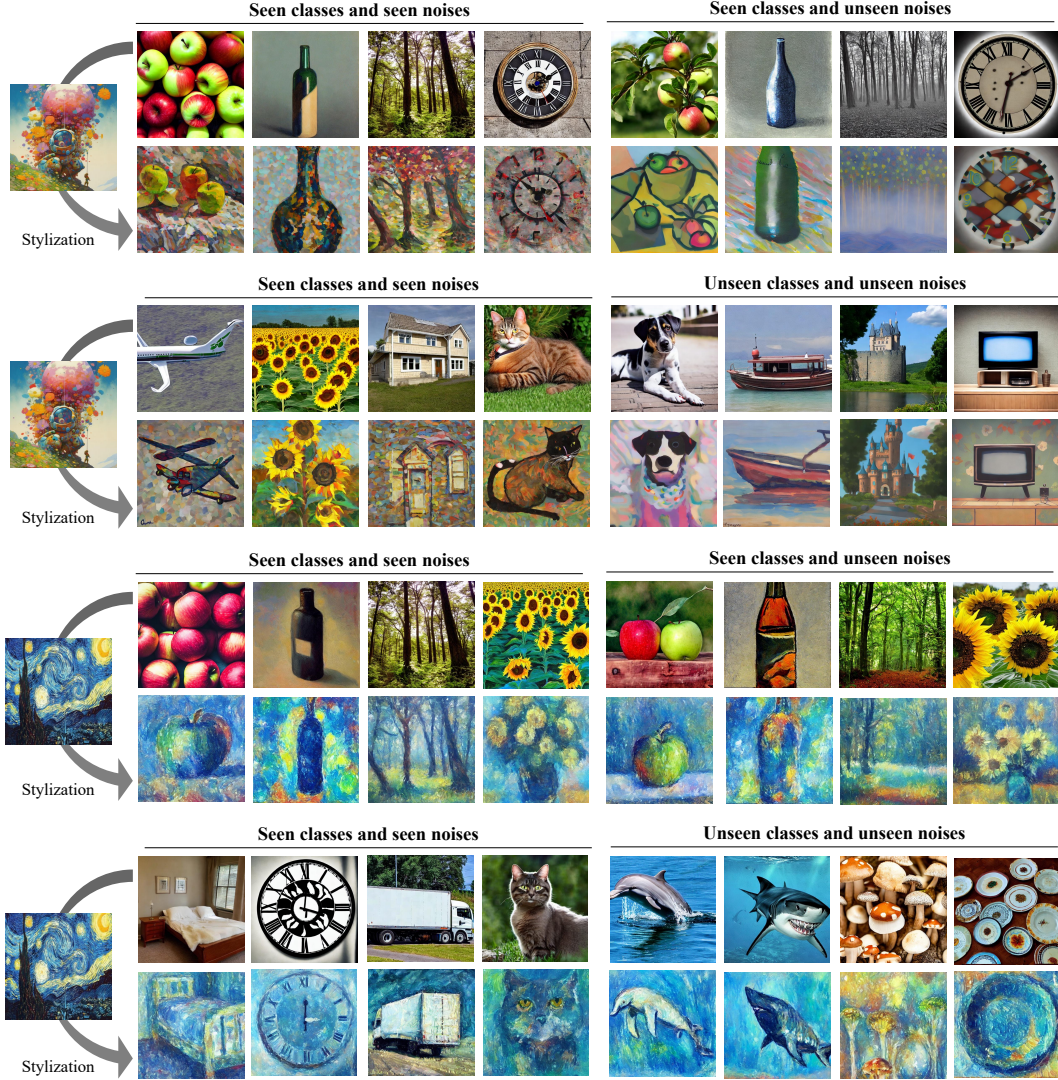


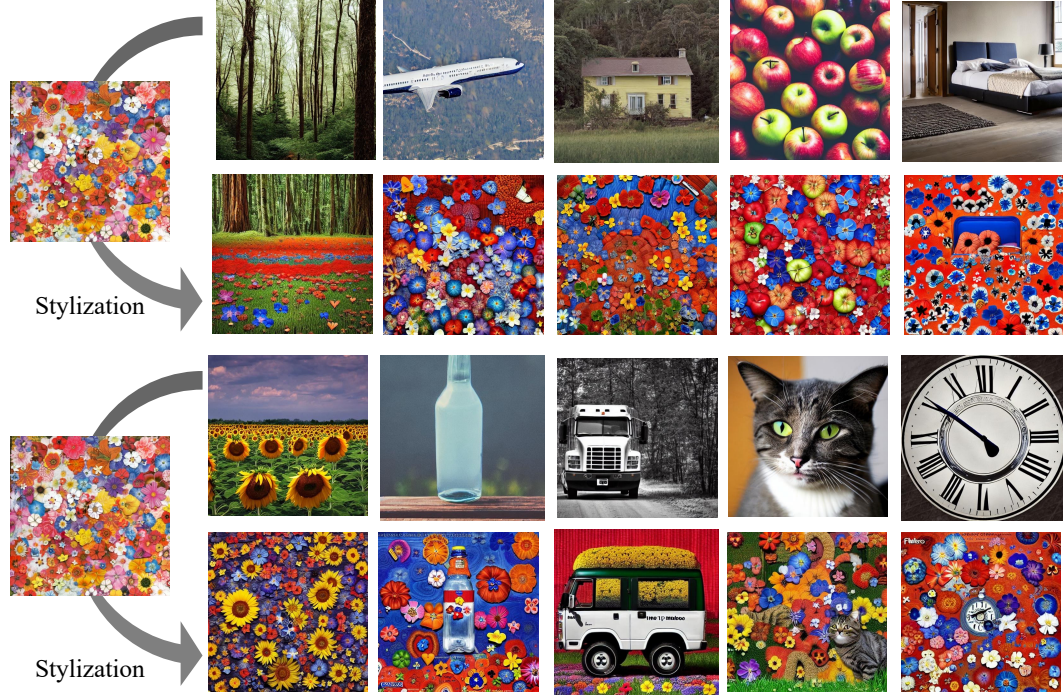
Figure 8: Stylization examples on other style images

Security Auditing under an ImageNet Classifier. To generate adversarial samples against an ImageNet classifier, we follow the implementation of classifier guidance generation of DPM¹¹ and use the publicly released checkpoints trained on the ImageNet 128x128 dataset to generate images in conditional manner. We adopt the pre-trained ResNet50¹² as our ImageNet classifier.

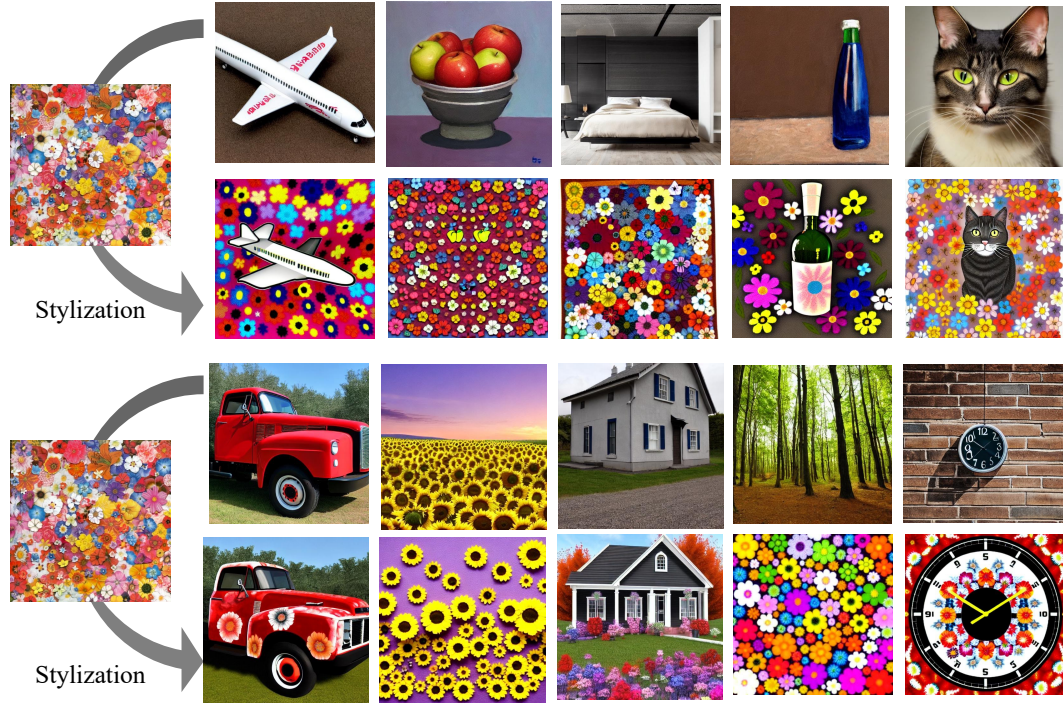
To generate adversarial examples, we first randomly choose an ImageNet class and set it as the class label for classifier guidance generation, and then we pass the generated images to the ResNet50 classifier. If the outputs of ResNet50 classifier are aligned with the chosen class label, we begin to do an adversarial attack by using AdjointDPM. For the adversarial attack, we adopt the targeted attack, where we choose a target class and make the outputs of ResNet50 close to the pre-chosen target class by minimizing the cross entropy loss. We also clamp the updated initial noise in the range of $[x_T - 0.8, x_T + 0.8]$ (i.e., set $\tau = 0.8$ in Sec. 4.3 to ensure that generated images do not visually change too much compared with the start images. We show more adversarial examples against the ImageNet classifier in Fig. 10. Besides, define the attack rate as the ratio between the number of samples with incorrect classification results after the attack and the total number of samples. We also

¹¹https://github.com/LuChengTHU/dpm-solver/tree/main/examples/ddpm_and_guided-diffusion

¹²<https://pytorch.org/vision/stable/models.html>



(a) Stylization examples generated by Textual Inversion.



(b) Stylization examples generated by DreamBooth.

Figure 9: In Textual Inversion, we generated the original images by using the prompt “A photo of a <object name>” and generated the style images by using the prompt “A photo of a <object name> in the style of <bengiles>”, where <bengiles> is our learned text embedding. In DreamBooth, we generated the original images by using the prompt “A <object name>” and generated the style images by using the prompt “A <object name> in the style of bengiles flowers”, where bengiles flowers is our input instance prompt. The original images and their corresponding stylized images use the same initial noises.

get the attack rate 51.2% by generating 830 samples from 10 randomly chosen classes. The class labels here we choose are [879, 954, 430, 130, 144, 242, 760, 779, 859, 997].



Figure 10: Adversarial examples against the ImageNet classifier. We show the originally generated images with their class names on the left; these images are correctly classified by ResNet50. On the right, we show the corresponding adversarial images which successfully mislead the classifier.

More Experimental Results on the NSFW Filter. In this case, we set $\tau = 0.9$. We follow the implementation of Stable Diffusion¹³ and set the loss function as the cosine distance between CLIP embeddings [23] of generated images and unsafe embeddings from [25]. In Fig. 11, we show two more adversarial examples against the NSFW filter.



Figure 11: Adversarial examples against the NSFW filter

A.4 Implementation of AdjointDPM on VP-SDE

In this section, we present the explicit AdjointDPM algorithm on VP-SDE and its implementation.

For VP-SDE, we have $f(t) = \frac{d \log \alpha}{dt}$ and $g^2(t) = \frac{d \sigma_t^2}{dt} - 2 \frac{d \log \alpha}{dt} \sigma_t^2$. Based on the definition of \mathbf{y}_t and ρ , we obtain

$$\mathbf{y}_t = \frac{\alpha_0}{\alpha_t} \mathbf{x}_t, \quad \rho = \gamma(t) = \alpha_0 \frac{\sigma_t}{\alpha_t} - \sigma_0.$$

We denote the timesteps for solving forward generation ODE as $\{t_i\}_{i=0}^N$, where N is the number of timesteps. Then based on this re-parameterization, we can show our explicit forward generation algorithm and reverse algorithm of obtaining gradients for VP-SDE in Algorithm 2 and Algorithm 3.

Implementation Details of AdjointDPM For the choice of α_t , σ_t , and sampling steps $\{t_i\}_{i=1}^N$, we adopt the implementation of DPM-solver¹⁴. Specifically, we consider three options for the schedule of α_t and σ_t , discrete, linear, and cosine. The detailed formulas for obtaining α_t and σ_t for each schedule choice are provided in [18, Appendix D.4]. The choice of schedule depends on the specific applications. We usually solve the forward generation ODE function from time T to time ϵ ($\epsilon > 0$ is a

¹³<https://github.com/huggingface/diffusers>

¹⁴<https://github.com/LuChengTHU/dpm-solver>

hyperparameter near 0). Regarding the selection of discrete timesteps $\{t_i\}_{i=1}^N$ in numerically solving ODEs, we generally divide the time range $[T, \epsilon]$ using one of three approaches: uniform, logSNR, or quadratic. The specific time splitting methods can be found in the DPM-solver. Subsequently, we obtain the generated images and gradients by following Algorithm 2 and Algorithm 3. To solve ODE functions in these algorithms, we directly employ the *odeint adjoint* function in the *torchdiffeq* packages¹⁵.

Algorithm 2 Forward generation by solving an ODE initial value problem

Input: model ϵ_θ , timesteps $\{t_i\}_{i=0}^N$, initial value \mathbf{x}_{t_0} .
 $\mathbf{y}_{t_0} \leftarrow \mathbf{x}_{t_0};$ ▷ Re-parameterize \mathbf{x}_{t_0}
 $\{\rho_i\}_{i=1}^N \leftarrow \{\gamma(t_i)\}_{i=1}^N;$ ▷ Re-parameterize timesteps
 $\mathbf{y}_{t_N} = \text{ODESolve}\left(\mathbf{y}_{t_0}, \{\rho_i\}_{i=1}^N, \epsilon_\theta\left(\frac{\alpha_t}{\alpha_{t_0}}\mathbf{y}_t, \gamma^{-1}(t), c\right)\right)$ ▷ Solve forward generation ODE
Return: $\mathbf{x}_{t_N} = \frac{\alpha_{t_N}}{\alpha_{t_0}}\mathbf{y}_{t_N}$

Algorithm 3 Reverse-mode derivative of an ODE initial value problem

Input: model ϵ_θ , timesteps $\{\rho_i\}_{i=1}^N$, final state \mathbf{y}_{ρ_N} , loss gradient $\partial L / \partial \mathbf{y}_{\rho_N}$.
 $a(\rho_N) = \frac{\partial L}{\partial \mathbf{y}_{\rho_N}}, a_\theta(\rho_N) = \mathbf{0}, z_0 = [\mathbf{y}_{\rho_N}, a(\rho_N), a_\theta(\rho_N)]$ ▷ Define initial augmented state.
def AugDynamics($[\mathbf{y}_\rho, \mathbf{a}_\rho, \cdot], \rho, \theta$) ▷ Define dynamics on augmented state.
return $[\mathbf{s}(\mathbf{y}_\rho, \rho, \theta, c), -\mathbf{a}_\rho^T \frac{\partial \mathbf{s}}{\partial \mathbf{y}}, -\mathbf{a}_\rho^T \frac{\partial \mathbf{s}}{\partial \theta}]$ ▷ Concatenate time-derivatives
 $[\mathbf{y}_{\rho_0}, \frac{\partial L}{\partial \mathbf{y}_{\rho_0}}, \frac{\partial L}{\partial \theta}] = \text{ODESolve}(z_0, \text{AugDynamics}, \{\rho_i\}_{i=1}^N, \theta)$ ▷ Solve reverse-time ODE
Return: $[\frac{\partial L}{\partial \mathbf{x}_{t_0}}, \frac{\partial L}{\partial \theta}]$ ▷ Return gradients

¹⁵<https://github.com/rtqichen/torchdiffeq>